CRYSTAL GROWTH & DESIGN

Article

pubs.acs.org/crystal

Biocompatible Alginate Microgel Particles as Heteronucleants and Encapsulating Vehicles for Hydrophilic and Hydrophobic Drugs

Huseyin Burak Eral,[†] Vilmalí López-Mejías,[†] Marcus O'Mahony, Bernhard L. Trout, Allan S. Myerson, and Patrick S. Doyle*

Novartis-MIT Center for Continuous Manufacturing and the Department of Chemical Engineering, Massachusetts Institute of Technology, 77 Massachusetts Avenue, E19-502b, Cambridge, Massachusetts 02139, United States

Supporting Information

ABSTRACT: Biocompatible materials that can control crystallization while carrying large amounts of active pharmaceutical ingredients (APIs) with diverse chemical properties are in demand in industrial practice. In this study, we investigate the utility of biocompatible alginate (ALG) hydrogels as a rational material for crystallizing and encapsulating model APIs that present drastically different solubilities in water. Acetaminophen (ACM) and fenofibrate (FEN) are utilized as the model hydrophilic and hydrophobic moieties, respectively. ALG hydrogels with different ALG concentrations (hence different mesh sizes) are utilized as heteronucleants to control the nucleation kinetics of ACM from solution. ALG hydrogels with smaller mesh sizes showed faster nucleation kinetics. We hypothesize that this behavior is due to the interplay between the polymer−solute interactions and the mesh-induced confinement effects. The loading of ACM into hydrogels by equilibrium partitioning is quantified and found to be inversely proportional to ALG concentration. For hydrophobic model APIs, loading via equilibrium partitioning is inefficient; hence, we suggest emulsion-laden hydrogels where emulsion droplets are encapsulated inside the hydrogel matrix. The incorporation of emulsion droplets inside hydrogels enables the high loading of the hydrophobic API leveraging the high solubility of the hydrophobic API in the dispersed emulsion droplets. By carefully choosing the emulsification method and the dispersed phase, we demonstrate significant loading (up to ∼80% w/w) and crystallization of the stable form of FEN. Our results provide new insights for designing biocompatible nucleation-active materials capable of carrying industrially significant amounts of water-soluble and insoluble APIs in the crystalline form.

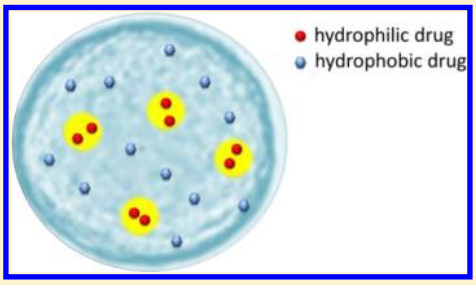

INTRODUCTION

Crystallization is omnipresent in nature and industrial practice, and is of particular significance to the chemical and pharmaceutical industry.[1,2] It is notoriously difficult to control and scale up as a significant portion of the crystallization process starts at foreign interfaces such as container walls, impurities, and dust. A promising direction for controlling crystallization is to target nucleation, a critical step in the process, by designing heteronucleant materials capable of influencing crystallization through selective interactions. However, in industrial practice, particularly in the pharmaceutical industry, compounds to be crystallized are diverse in chemical structure and hence in physicochemical properties such as solubility. Therefore, the heteronucleant materials in industrial practice should be biocompatible and capable of controlling crystallization, while carrying industrially relevant amounts of both hydrophobic and hydrophilic compounds in crystalline form.

Controlling nucleation of active pharmaceutical ingredients (APIs) with heteronucleants remains challenging due not only to the diverse chemical nature of APIs but also due to the sensitivity of the nucleation barrier to experimental conditions[3] and the physical properties of the interface inducing nucleation.[4,5] Although many attempts have been made to control nucleation by gaining understanding of the experimental conditions, the scarcity of investigations studying the role that interfacial properties play during nucleation may hinder our capacity to rationally design heteronucleants; to this end, this Article aims to provide new insights for designing biocompatible nucleation-active materials capable of carrying industrially relevant quantities of water-soluble and insoluble APIs in the crystalline form.

Considerable progress has been made in understanding the role of interfaces on nucleation. Among the proposed mechanism, epitaxy and functional group chemistry has been successful in describing nuclei formation on surfaces such as self-assembled monolayers,[6−9] molecular single-crystal surfaces,[10] and crystalline polymer surfaces.[5] Interfaces can influence nucleation via polarization matching in cases where both the interface and the crystal exhibit a net dipole interaction[11,12] as well. Furthermore, the geometry and the porosity of the interface at length scales relevant to nucleation are shown to affect not only nucleation kinetics[13,14] but also polymorphism.[15−17] Despite the considerable strides made with the aforementioned crystalline interfaces, their material properties

Received: February 18, 2014

   dx.doi.org/10.1021/cg500250e | Cryst. Growth Des. XXXX, XXX, XXX−XXX

are not easily adjustable. Noncrystalline materials such as hydrogels offer a more promising option as their structure, topology, interfacial, and mechanical properties can be easily tuned with a wide range of fabrication methods. In particular, synthetic poly(ethylglycol) (PEG) hydrogels with tunable microstructures have been demonstrated to be exceptional materials for controlling nucleation kinetics of hydrophilic APIs.[18−20] The hydrogels influence nucleation kinetics through two distinct mechanisms, confinement[21−25] and favorable solute−polymer interactions.[26] In contrast to rigid nanoporous materials previously reported for studying nucleation under confinement,[15,16,27] soft polymer gels are solvated. Therefore, they can swell and concentrate solute molecules within the polymer network via thermodynamic partitioning driven by favorable polymer−solute interactions.

Despite their ease of fabrication and utility as model hydrogels, previously used PEG hydrogels are prepared by free radial polymerization[26]—a process generally avoided in the pharmaceutical industry. In an effort to create pharmaceutically acceptable nucleation active hydrogels capable of carrying APIs of distinct water solubilities, we turn to alginate (ALG), a biocompatible polysaccharide widely used in the food and pharmaceutical industry.[28−32] ALG, isolated from brown algea, is a linear copolymer, consisting of *b*-D-mannuronic acid (M) and its C-5 epimer, *a*-L-guluronic acid (G), arranged in a block-wise pattern. Gel formation can be induced by lowering pH or by adding various divalent cations, in particular Ca^{2+}, which cross-links a pair of G blocks within the alginate chains. Despite its utility for carrying hydrophilic drugs,[33] ALG is hydrophilic in nature; hence it cannot be loaded with significant amounts of hydrophobic drugs.[32]

It is important to note that a significant fraction of pharmaceuticals are of hydrophobic nature and do not lend themselves effectively to thermodynamic partitioning.[34] Considerable efforts have been placed on synthesizing/modifying hydrogels capable of carrying hydrophobic moieties.[35,36] For instance, hydrogels can be modified by copolymerizing or grafting hydrophobic units to hydrophilic polymer network, effectively creating hydrophobic mesoscale regions.[37] These methods are not effective for loading high weight percentages of APIs into the hydrogel. Recently, emulsion-laden hydrogels containing nano-[38] and microemulsions[39,40] have been used for delivery\controlled release of model hydrophobic cargo.[41−43] However, the focus of these studies has been on controlled release, and not on crystallization.

In an effort to develop a biocompatible material capable of controlling crystallization and carrying large amounts of the APIs of diverse chemical nature, we investigate the utility of ALG hydrogels as heteronucleants and encapsulation vehicles to carry APIs in crystalline form (Figure 1). For model hydrophilic APIs, we investigate ALG hydrogels with different mesh sizes. For hydrophobic APIs, we developed emulsion-laden hydrogels leveraging the ability of lyophilic emulsion droplets to dissolve and carry large amounts of hydrophobic APIs. We investigate ALG hydrogels as heteronucleants for the model hydrophilic API (acetaminophen, ACM); the mesh size (ξ) of the hydrogel network is systematically varied by manipulating the polymer concentration. ACM nucleation kinetics from solution and ability to encapsulate of the API into the hydrogel through equilibrium partitioning are quantified as a function of mesh size. We demonstrate that emulsion-laden hydrogels can carry large amounts of fenofibrate (FEN) and can crystallize the stable form of FEN. Through careful choice

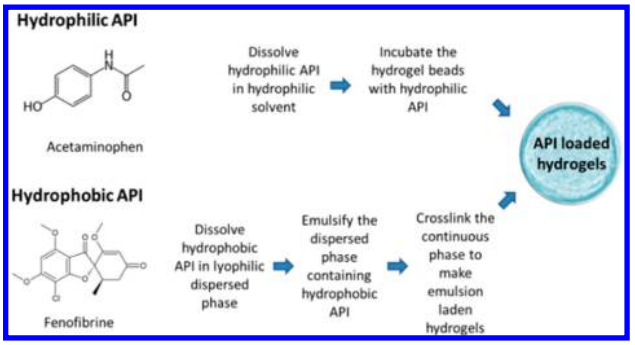

Figure 1. Illustration of the two routes developed for formulating hydrophobic and hydrophilic API loaded hydrogels.

of the dispersed phase and emulsification methods, we developed optimal formulations of emulsion-laden ALG hydrogels that are capable of carrying adjustable and industrially relevant amounts (up to 80% w/w) of FEN in crystalline form.

MATERIALS AND METHODS

Materials. Sodium alginate (Na−ALG) isolated from brown algae was purchased from Sigma Aldrich (CAS no. 9005-38-3). The weight average molecular mass was between 80 000 and 120 000. The mannuronic acid and guluronic acid ratio was 1.56. Compounds $CaCO_3$ (mean particle size 10 μm, CAS no. 471-34-1), sodium chloride (NaCl, CAS no. 7647-14-5), 4-(2-hydroxyethyl)piperazine-1-ethanesulfonic acid, *N*-(2-hydroxyethyl)piperazine-*N*′-(2-ethanesulfonic acid) (Hepes, CAS no. 7365-45-9), and glucono-δ-lactone (GDL, CAS no. 90-80-2) were purchased from Sigma-Aldrich. Acetaminophen (ACM, CAS no. 103-90-2) and fenofibrate (FEN, CAS no. 49562-28-9) were purchased from Sigma-Aldrich.

Preparation of Na−Alginate Solutions. Na−alginate solutions were prepared by dissolving the polysaccharide powder in aqueous deionized water with NaCl 0.3 M, Hepes 20 mM (pH 7.4) at final ALG concentrations of 2, 4, 6, 8, 10, and 12% w/v. The homogeneity of solution was assured by rigorous magnetic stirring.[44]

Preparation of Crystallization Solutions for Induction Time Measurements. The ACM solution was prepared by dissolving ACM powder (10 g) in 50 mL of ethanol at 65 °C. The FEN solutions were prepared by dissolving powdered FEN (450 mg and 15 g) in heptane (50 mL) and ethyl acetate (25 mL) at 65 °C.

Preparation of Disk-Shaped ALG Hydrogels for Rheological Measurements. For rheological measurements, Ca^{2+} saturated disk shaped hydrogels were prepared by two stage cross-linking. In the first stage, Na−ALG solutions were mixed by an inactivated form of Ca^{2+} ($CaCO_3$, 20 mM) followed by the addition of the slowly hydrolyzing glucono-δ-lactone (GDL), maintaining a ratio $[GDL]/[Ca^{2+}] = 2$. The suspension was degassed prior to the addition of GDL to avoid bubble formation. Removing bubbles entrapped in Na−ALG solution for high weight Na−alginate solutions was required to get clean measurements. The hydrogels were cured in a Petri dish (35 mm diameter) for 24 h to get cylindrically shaped hydrogels. In the second phase of curing, 3 mL of a 6% w/v aqueous $CaCl_2$ was added to hydrogels from previous cross-linking step. The hydrogels were cured for 48 h prior to rheological measurement, ensuring that Ca^{2+} saturates all of the possible binding sites. The final dimensions of the hydrogels used for rheological determination were 3 mm height and 20 mm diameter.

Preparation of Spherical ALG Hydrogel Beads. Na−ALG solutions prepared as reported were dripped into a gelling bath containing 6% w/v $CaCl_2$. The ALG gel beads were aged for 24 h in the gelling solution prior to analysis. The average diameter of the beads was 750 μm (COV, coefficient of variation: 8%).

Rheological Measurements. Rheological characterization of disk-shaped ALG hydrogels was performed with controlled stress rheometer TA 2000 with a plate and plate geometry (20 mm) and operating at 20 °C. To avoid evaporation, the measurements were

dx.doi.org/10.1021/cg500250e | *Cryst. Growth Des.* XXXX, XXX, XXX−XXX

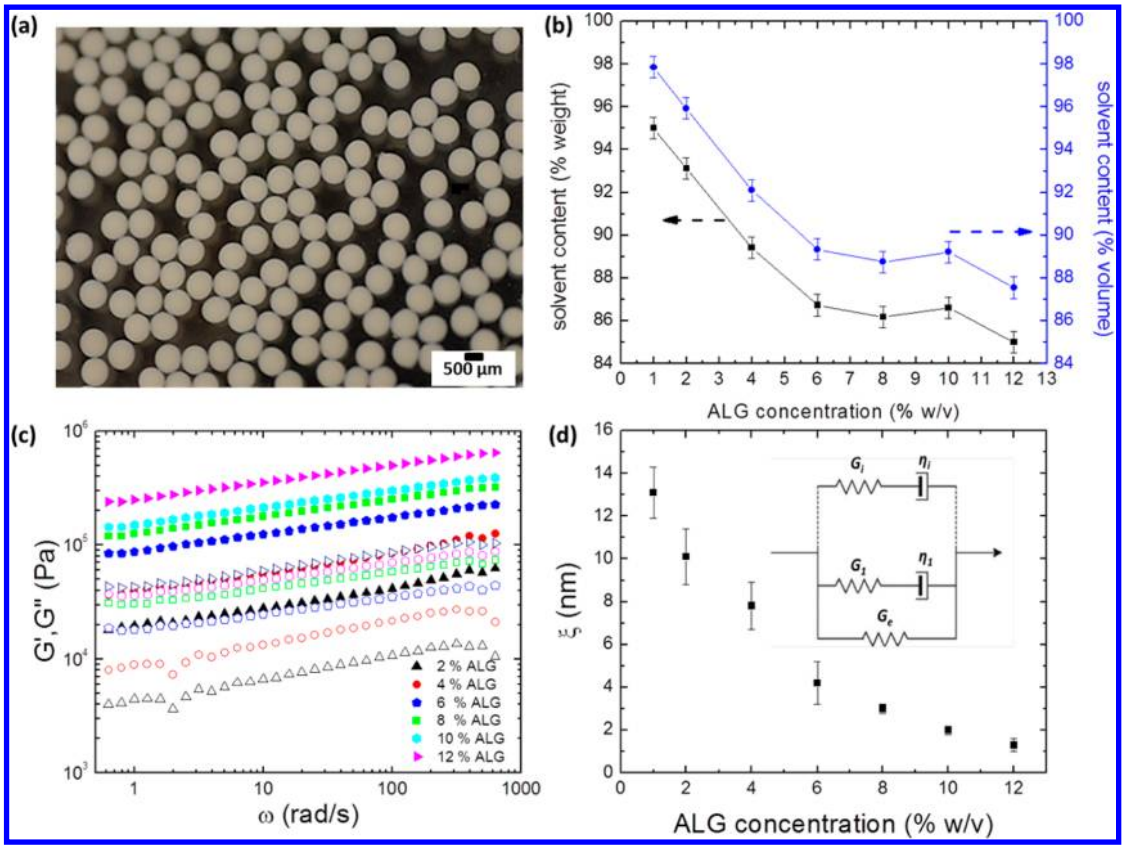

Figure 2. (a) Optical micrographs of 4% w/v ALG hydrogel beads with mean size 760 μm with standard deviation 52 μm (coefficient of variation: 0.08). (b) The solvent content by weight (left-hand axis) and by volume (right-hand axis) calculated from evaporation experiments. (c) Rheological measurements for ALG hydrogels prepared with different Na−ALG concentrations. (d) The average mesh size and mechanical illustration of Maxwell model for calculating mesh size (inset).

performed with a solvent trap. Sand paper was used to eliminate wall slip. To identify the optimum gap height that eliminates the wall slip and the excessive gel squeezing (reflecting in the alterations of polymeric network properties), the gap was reduced systematically while executing a series of short frequency sweeps with strain = 0.05%. The selected gap maximizing the value of the elastic modulus G' was reported. We also ensured that the normal force applied on samples prior to measurement does not exist 1 N for each measurement. For each hydrogel of a given weight fraction, the linear viscoelastic range was identified by a strain sweep with increasing strain stress ($0.01\% < \gamma < 1000\%$) with frequency (ω) 20 rad/s. The strain chosen to perform the frequency sweep was an order of magnitude lower than yield strain of the weakest gel. The frequency sweeps were performed at 0.05% strain that was 2 orders of magnitude lower than the yield stress. All tests (stress and frequency sweep) were performed in triplicate.

Procedure for Synthesizing Emulsion-Laden Hydrogels. The procedure for synthesizing emulsion-laden hydrogel capable of carrying hydrophobic API can be divided into three steps: (i) dissolving the API in dispersed phase, (ii) emulsifying the API carrying dispersed phase in continuous phase containing the ALG biopolymer, and (iii) cross-linking ALG to encapsulate emulsion-laden hydrogel beads (Figure 1).

EMULSIFICATION FOR PREPARING EMULSION-LADEN HYDROGELS

Magnetic Stirring. In magnetic stirring emulsification, the dispersed phase with dissolved API was slowly dripped into the continuous phase containing surfactant in a 100 mL flask as a magnetic stirrer emulsified the dispersed phase droplets at 1000 rpm. For all of the formulations, a 1% by volume Pluronic F-68 (polyoxyethylene(PEO)−polyoxypropylene(PPO) block co-polymer) purchased from Sigma Aldrich was used. The volume fraction (φ) of the dispersed oil phase was set by adjusting the volume of dispersed phase dripped into the flask relative to the volume of continuous phase containing 2% w/v ALG.

High Pressure Homogenization. In high pressure homogenization (HPH), a pre-emulsion solution prepared by magnetic stirring was emulsified by pumping the solution through a homogenization valve that varies its diameter with respect to the applied pressure. The applied pressure can be varied to achieve pressure drops between 5 and 25 kpsi across homogenization valve that directly influences the size and polydispersity of emulsified droplets.[38] For the emulsions utilized in this study, high HPH of the pre-emulsion was carried out using an Avestin Emulsiflex-C3 homogenizer operating at 15 kpsi. Number of passes was set to $N = 10$.

Method of Cross-Linking Na−ALG Containing Emulsions. Na−alginate solutions containing emulsion at desired volume fraction were dripped into a gelling bath containing 6% w/v $CaCl_2$. The ALG concentration was defined as the concentration in the continuous phase, and all of the samples prepared were set to 4% w/v. The ALG gel beads were aged for 24 h in the gelling solution prior to analysis to completely cross-link Na−ALG.

Characterization of Emulsions and Emulsion-Laden Hydrogels. The size of emulsion droplets prepared by magnetic stirring was characterized by inverted microscope (Axiovert 200, Zeiss). Nanoemulsion droplet sizes were measured via dynamic light scattering using a Brookhaven Instruments BI-200SM multiangle apparatus. Samples were

dx.doi.org/10.1021/cg500250e | Cryst. Growth Des. XXXX, XXX, XXX−XXX

diluted to φ = 0.0005 in deionized water. Autocorrelation functions were measured at a scattering angle of 90° and a temperature of 25 °C. Cumulant analysis was conducted on the data acquired to obtain the hydrodynamic droplet diameter distribution. Coefficient of variation (COV) was defined here as the variance of the size distribution relative to the mean size. We visualized the emulsion-laden hydrogels by a environmental scanning electron microscope (ESEM) FEI/Philips XL30 in hydrated form. Scanning electron microscopy (JEOL 5910 General Purpose SEM) was used to analyze the surfaces of the dried particles.

CHARACTERIZATION OF ALG HYDROGELS

We characterized ALG hydrogels in terms of solvent content and mesh size: (i) the solvent content is quantified by evaporation measurements, and (ii) the mesh size is characterized by rheological measurements. For the evaporation measurements, spherical ALG beads (Figure 2a) are used, whereas for rheological measurements disk-shaped hydrogels are prepared due to the requirements of the rheometer. It is important to note that both hydrogel geometries are Ca^{2+}-saturated to completely cross-link ALG hydrogels. The evaporation measurements provided information on the weight ratio of the solvent to the hydrogel beads, which is then converted to a volume ratio of hydrogel as the volume of the bead is known a priori. The hydrogel beads (approximately 20 beads) are first pat dried, weighed, and then an optical image is taken to estimate the size (Figure 2a). The beads are placed in a vacuum oven 120 °C overnight to evaporate the solvent. The weight change between the hydrated and dried hydrogel is recorded as the weight of the evaporated solvent. The weight of the evaporated solvent is converted to the volume evaporated, as the density of the solvent is known. The weight and the volume ratio of the solvent to the ALG are given in Figure 2b. All of the measurements are performed in triplicate.

The characterization of mesh size for ALG hydrogels with different ALG concentrations is performed by oscillatory rheology. The disk-shaped ALG gels at different ALG concentrations, 2, 4, 6, 8, 10, and 12% (w/v), are prepared in calcium-saturated conditions, and their rheological response is recorded (Figure 2c). In all ALG concentrations considered, the storage (G') modulus is monotonous and significantly higher than the loss modulus (G''), indicating strong gel behavior. Frequency sweep measurements at a fixed strain (0.05%) are modeled in terms of the generalized Maxwell model.[45] The model utilized is composed of a sequence of elements in parallel (spring and dashpot) to which an additional spring has been added (Figure 2d and Supporting Information). The use of the generalized Maxwell model and rubberlike elasticity theory allows determination of the shear modulus, G, and average mesh size (ξ).

As the mechanical characterization is performed in the linear viscoelastic region, the response of the ALG network is dominated by entropic contribution.[46] The average mesh size can be estimated as $\xi = (6\alpha RT/\pi N_A G)^{1/3}$ from the shear modulus G, where N_A is Avogadro's number, T is temperature, and α is a dimensionless constant.

To estimate the prefactor, α, we turn to previous work performed in low-weight-fraction ALG gels where mesh size is determined via various techniques and compared to rheological characterization.[44] In the work of Turco et al.,[44] α is estimated to be 16.1 by comparing the rheological, TEM, and NMR measurements for ALG concentrations less than 4%. We expect that that this front factor applies to our measurements with higher ALG concentrations as the front factor accounts for the deviations from point-like, compressible cross-links of ideal rubber as described by the Flory theory.[47] Furthermore, the mesh size values calculated agree well with the previously reported values at lower ALG concentrations[48] (Supporting Information).

Measuring the Partitioning Coefficient of Hydrophilic API. Prior to insertion into the saturated solution (200 mg/mL ACM in ethanol at 27 °C), the hydrogel beads previously immersed in ethanol are pat-dried, weighed, and imaged for size determination. The beads are left to equilibrate over 3 days to ensure the equilibrium partitioning of API between the continuous phase and the hydrogel. The hydrogels are later pat-dried, weighed, and imaged again. The difference in weight before and after the equilibration is attributed to the API in the hydrogel. Because the mass of API in hydrogels, average diameter of beads, and the number of beads are known, the concentration of API is calculated ($C_{\text{API in hydrogel}}$). The concentration of API in continuous phase ethanol ($C_{\text{API in ethanol}}$) is calculated as the initial mass of API in ethanol minus the mass of API in the hydrogels divided by the initial volume of ethanol. The partitioning coefficient is calculated as the ratio of two concentrations $\kappa = ((C_{\text{API in hydrogel}})/(C_{\text{API in ethanol}}))$ given in Figure 3a. We observed similar results when we measured the partitioning coefficient using the remaining amount of ACM in solvent.

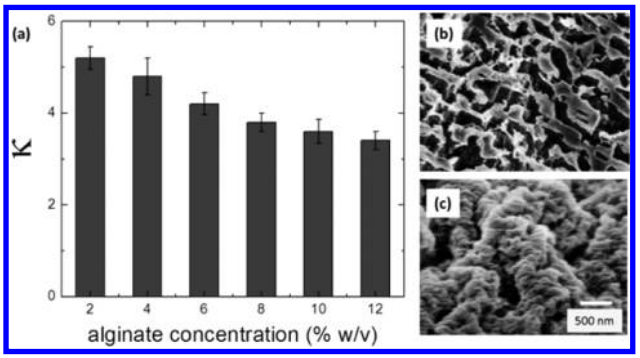

Figure 3. (a) Partition coefficient of ACM for different ALG concentrations. (b) Cross section of a 4% w\v ALG bead first pat-dried, then dried in an oven at 120 °C overnight prior to SEM imaging and (c) cross section of a 4% w\v ALG bead loaded with ACM.

Procedure for Dissolution Profile of Hydrophobic API in the Emulsion-Laden Hydrogels. The release kinetics of FEN from the emulsion-hydrogels was carried out at 37 °C, while the solution is stirred at 75 rpm The dissolution medium was prepared by adding 0.72% w/v SDS to aqueous media at pH 6.8.[49] Three samples of 2 mL were taken from the 600 mL vessel at each time point, and UV absorption was recorded as a function of time. The total amount of dried emulsion-laden hydrogels prepared with ethyl acetate as dispersed phase was 250 mg. The solvent ethyl acetate was evaporated at 50 °C overnight.

Procedure for Measuring Loading of Hydrophobic API in the Emulsion-Laden Hydrogels. For hydrophobic drugs, the dispersed phase is emulsified in nano- and micrometer-size droplets using heptane and ethyl acetate as solvent to load the drugs inside the ALG particles (Figure 7a). The emulsified solution is added to the ALG solution of various concentrations, and these are cross-linked in situ in a calcium

dx.doi.org/10.1021/cg500250e | Cryst. Growth Des. XXXX, XXX, XXX−XXX

chloride solution. The emulsion-laden hydrogels are synthesized with different emulsion volume fractions ranging from 10% to 50%. For each measurement of a given volume fraction (φ), two batches of emulsion-laden hydrogels are prepared with the same method of emulsification followed by cross-linking: preparing a reference batch without API and a test batch with API. Both batches containing approximately 200 mg of ALG beads are pat-dried and weighed. The samples containing both batches are placed in a vacuum oven and dried over 2 days above the boiling point of dispersed phase at 140 °C (boiling point of heptane 98 °C, ethyl acetate 77.1 °C at 1 bar). Initially heptane was used as the continuous phase; later, in an effort to maximize the loading, ethyl acetate was used. The solubility of FEN in ethyl acetate is considerably larger than that in heptane (9 and 600 mg/mL). Loading is defined as the difference in weight between the hydrogels containing the API-carrying emulsions and control batch without the API divided by the weight of the API-carrying emulsion-laden hydrogel on dry solute basis as follows:

$$\text{loading\%} = \frac{W_{\text{API carrying emulsion-laden hydrogel}} - W_{\text{reference emulsion-laden hydrogel}}}{W_{\text{API carrying emulsion-laden hydrogel}}} \times 100$$

To estimate the variation in loading and significance of variation, we repeated loading measurements in 10 replicates. ESEM images confirm the presence of the emulsified droplets inside the ALG particle (Figure 7b,c). Additionally, TGA analysis showed that when hydrophobic drugs are encapsulated through HPH or magnetic stirrer emulsification, the residual solvent content is less than that of the method utilized for hydrophilic drugs (Supporting Information).

RESULTS AND DISCUSSION

We investigate ALG hydrogels as heteronucleants, and to encapsulate crystalline materials. To investigate the potential use of ALG hydrogels to influence nucleation, ALG particles of different concentrations and hence mesh size are utilized as heteronucleants during crystallization from solution. ACM was crystallized using ethanol as a solvent (Figure 4). The solution

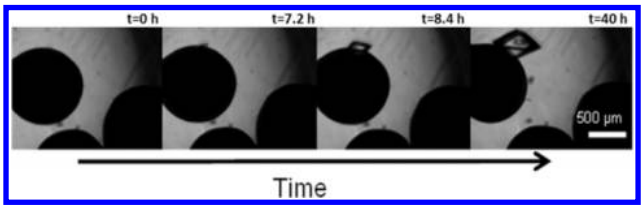

Figure 4. Optical micrographs from time-lapsed nucleation induction time experiments. ACM crystals grow in contact with ALG particles from a supersaturated ethanol solution at 10 °C.

(200 mg/mL) is undersaturated at room temperature and saturated (S = 1.5×) at 10 °C. Seventy-eight vials are prepared in total. The effect of crystal nucleation on five ALG concentrations, 4%, 6%, 8%, 10%, and 12%, is investigated using 13 vials for each concentration. Each 1 mL vial contained 4−8 ALG particles of a particular concentration. About 750 μL of the crystallization solution is delivered to each vial. Additionally, 13 vials that did not contain any ALG particles are prepared as controls. The samples were crash cooled from 65 to 10 °C to achieve a 1.5× supersaturated solution. The heating and cooling procedures were repeated to provide statistically significant data for the 78 samples for each ALG concentration. The crystal nucleation induction time for the vials was monitored continuously with an inverted microscope to determine the average induction time of nucleation. The onset of each crystallization event was detected optically; when the first crystal was observed the frame number was recorded. Frames were taken at 5-min intervals. The average nucleation induction time, τ, was determined from a statistical analysis of the induction time data, based on the knowledge that nucleation follows a Poisson distribution,[50] $P(t) = e^{(-t/\tau)}$, where P is the probability that no nucleation event occurs within time t. The total number of vials as a function of time was also monitored during the experiment.

Ranking the average induction time values for the different ALG concentrations employed as heteronucleants (Table 1)

Table 1. Summary of Average Induction Time (τ) Measurements for the ALG Particles of Different Concentrations Used as Heteronucleants during the Crystallization of ACM from a Supersaturated Ethanol Solution at 10°C

sample	τ (h)	error (h)	linearity
control	15.3	0.31	0.99
4% ALG	24.7	1.4	0.92
6% ALG	12.8	0.23	0.97
8% ALG	16.5	0.50	0.95
10% ALG	9.5	0.18	0.98
12% ALG	7.7	0.10	0.99

shows that induction time decreases with increasing ALG concentration. These results can be explained as the interplay of mesh-induced confinement and favorable solute−polymer interactions. A mechanistic explanation can be constructed thinking of these effects separately. Assuming the polymer−solute interaction is not varying for different ALG concentrations, the induction time is expected to increase with increasing ALG concentration due to decreasing mesh size (Figure 2d). The hydrogel mesh can be thought of as a container (of volume ξ^3) holding a constant concentration. With decreasing mesh size, that is, nucleation volume, the number of molecules attempting to form critical nuclei decreases, and hence induction time increases. However, thinking about only polymer−solute interaction, assuming mesh size is constant, produces an opposite effect. Solute−polymer interactions are expected to get stronger with increasing ALG concentration. In other words, the number of polymer chains that solute API encounters per volume increases (with increasing ALG concentration), leading to faster nucleation kinetics and hence smaller induction times.[18,20,26] Putting mechanistic explanations of the two effects together, we can explain the observed trend. As the ALG concentration increases, the inhibiting volume effect of mesh size is counteracted by increasing solute−polymer interactions leading to faster nucleation kinetics. These observations are in accordance with previously published results.[20,26]

Furthermore, at low ALG concentrations (<6%), the presence of ALG particles tends to inhibit nucleation kinetics with respect to bulk (control in Table 1), whereas at high ALG concentrations (>8%), the presence of ALG hydrogels as heteronucleants tends to promote nucleation of ACM from solution. We explain this behavior with two possible scenarios:

dx.doi.org/10.1021/cg500250e | Cryst. Growth Des. XXXX, XXX, XXX−XXX

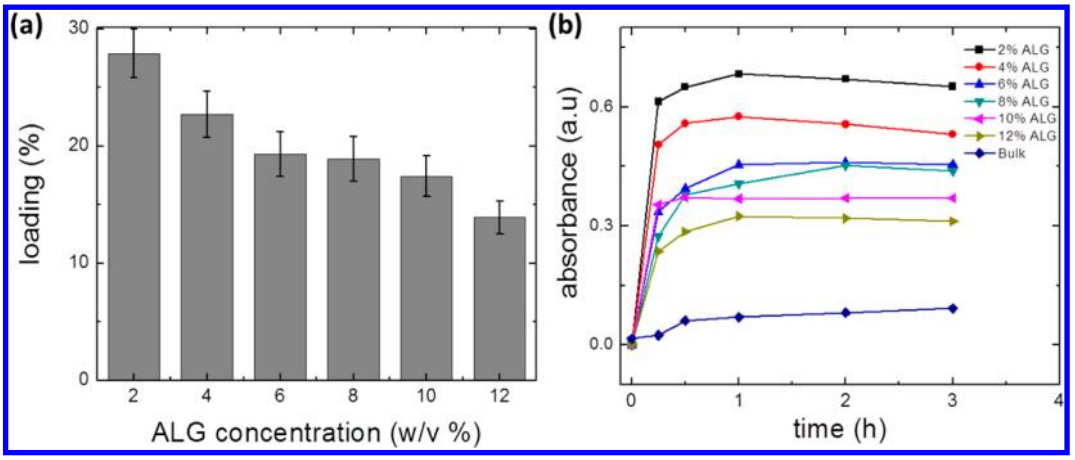

Figure 5. (a) ACM loading in hydrated hydrogels calculated by equilibrium partitioning for various ALG concentrations. (b) UV−vis absorbance measurements for ACM released from the ALG particles as a function of time in water.

(i) the absence of solute−polymer interactions in control, and (ii) the gradient of partitioning coefficient with respect to ALG concentration. The control measurements without ALG hydrogels can be thought of as a hypothetical hydrogel with large mesh size absent solute−polymer interactions. The absence of solute−polymer interaction might counteract the nucleation time enhancement due to large mesh size, hence leading to intermediate induction times. The other working hypothesis is attributed to the gradient of the partitioning coefficient. At low ALG concentrations (<6%), due to the relatively large partitioning coefficient (κ), the concentration of solute in continuous phase (Figure 3) is lower than that in the control, and hence larger induction times than for the bulk are observed. As our induction time measurements are more likely to capture crystals growing on the surface of hydrogel than ones deeply engulfed and possibly trapped in the hydrogel, the concentration in the bulk might directly influence the nucleation kinetics. Such behavior is not observed in previous studies of nucleation kinetics of ACM in the presence of hydrogels where partitioning coefficient is reported to be constant for different mesh sizes used.[18−20,26,51] As the characteristic time for ACM to diffuse into hydrogels is on the order of minutes, we believe ACM in hydrogels is in equilibrium with the ACM in the surroundings (Supporting Information).

To determine the potential use of ALG particles to encapsulate industrially relevant amounts of hydrophilic drug materials, the loading capacities of the ALG hydrogels with varying mesh sizes are tested via incubating API with the hydrogels. ACM is used as a model compound for this investigation. In this method, ALG particles are equilibrated in a saturated solution (200 mg/mL ACM in ethanol at 27 °C). At the end of the equilibration time, solid ACM remaining in the solution indicates that the system has reached equilibrium and no more partitioning into the ALG matrix will occur. The particles are washed with iced water and filtered. Scanning electron microscopy (SEM) is used to corroborate that the drug materials have been deposited inside the particle. A cross section of an ALG particle in which no drug product has been loaded, that is, control (Figure 3b), and another cross section of an ALG particle in which drug product has been loaded using the solvent exchange method are shown in Figure 3c.

To determine the amount of drug loaded, a known amount of the ALG particles was transferred to a known amount of solvent (water) and stirred at a constant temperature. The dissolution or release of the drug is monitored over time using UV−vis spectrometry, and the concentration of the drug at equilibrium is determined using its absorbance. It is observed that at lower ALG compositions the amount of drug loaded is more than twice the amount loaded at higher ALG concentrations (Figure 5). This effect might be due to the larger average mesh size of the lower ALG concentrations and also supports the findings with regards to the solute partition coefficient, which decreases with increasing ALG concentration.

Following the equilibrium partitioning procedure, the loaded ALG particles are analyzed to determine the solvent retained, a very important parameter in pharmaceutical formulations. Thermogravimetric analysis (TGA) is used to determine the solvent loss as a function of temperature. It is observed that for lower ALG concentrations, the percent weight loss is higher when the ALG beads are heated between 40 and 200 °C, indicating a higher percentage of solvent (ethanol and water) entrapped inside the pores of these hydrogels. At higher ALG concentrations, the percent weight loss is lower within the same temperature range, indicating that lower amounts of solvents (ethanol and water) remained inside the particles after they are loaded with the drug (Supporting Information). To reduce the solvent content without having to vacuum-dry the loaded samples, which would change the porosity and dissolution behavior of the encapsulated drug material, the ALG particles are directly compressed into tablets. About 250 mg of ALG particles are pressed with a 6-mm tablet maker to form a tablet (Supporting Information). TGA analysis is performed to determine the solvent content in the tablet. Thermograms showed that in the pressed ALG particles, the percentage weight loss is reduced by about 30%, indicating that most of the solvent was removed by direct compression (Supporting Information). Moreover, the 15% weight loss occurring initially in the thermogram of the loaded and compressed ALG particles corresponds to the drug loaded, which is about 17% when determined by equilibrium partitioning.

To determine if the drug material encapsulated in the ALG particle is crystalline or amorphous, powder X-ray diffraction (PXRD) analysis is employed. Diffractograms of the various loaded ALG beads of different concentrations suggest that all of the loaded material is crystalline (Figure 6). In general, smaller and lower numbers of diffraction peaks are observed in the high percent ALG particles than in the lower percent ALG particles.

dx.doi.org/10.1021/cg500250e | Cryst. Growth Des. XXXX, XXX, XXX−XXX

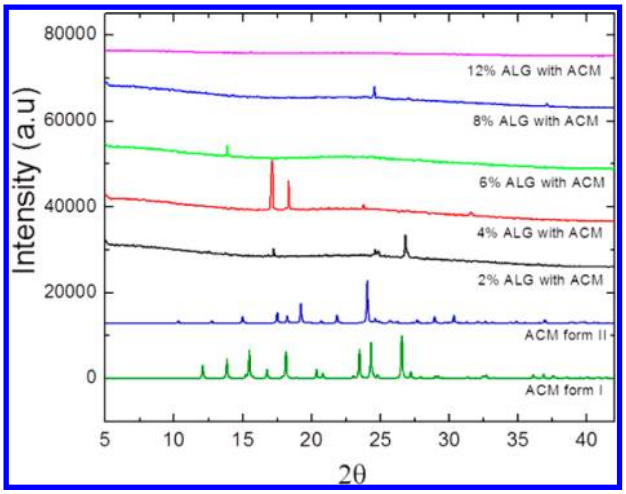

Figure 6. Experimental PXRD of loaded ALG particles at different concentrations, indicating that crystals of ACM form I have been encapsulated into the ALG particles.

This phenomenon might be due to the smaller size of the pores at higher ALG concentrations, which might lead to the presence of submicrometer size crystals that would be harder to detect by this technique. Moreover, PXRD indicates that at all ALG concentrations used in the encapsulation studies, the thermodynamically stable form of ACM, form I, is obtained.

By carefully selecting the material properties and the production techniques, we investigate the utility of emulsion-laden hydrogels (Figure 7) in carrying and crystallizing the

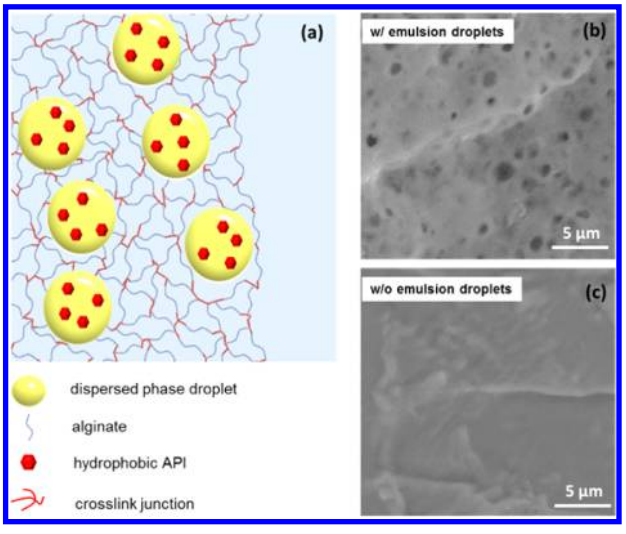

Figure 7. (a) Illustration showing emulsion-laden hydrogels loaded with hydrophobic API, fenofibrate (FEN). (b) Cross section of environmental scanning electron microscopy (ESEM) image of ALG hydrogels with emulsion droplets and (c) without emulsion droplets serving as control for panel (b). The continuous phase contains 2% ALG, and the volume fraction of the dispersed phase is 30% (v/v) FEN in heptane.

model hydrophobic API, FEN, and their potential as biocompatible final dosage formulations. We first investigate which solvents can be used and trapped inside hydrogels. The solvents to be used must satisfy the following criteria: (i) they have to be chosen from pharmaceutically acceptable organic solvents; (ii) they should dissolve large amounts of model hydrophobic APIs; and (iii) they should be amenable to emulsification and encapsulation within hydrogels. We identified heptane (HEP) and ethyl acetate (EA) as potential candidates due to their pharmaceutically acceptable nature. We studied their emulsification with different methods and their ability to act as hydrophobic API carrying liquid pockets within hydrogels. As emulsions trapped in hydrogel matrix provide a more favorable environment for FEN to partition as compared to the surrounding aqueous environment, we expect strong partitioning of FEN within emulsion droplets as only a small fraction of FEN can escape to aqueous environment (see the Supporting Information for a more detailed discussion).

First, we investigate which emulsification method is suitable for our purpose on the basis of loading. The emulsion-laden hydrogels with heptane as the dispersed phase are synthesized as described before with different emulsion volume fractions ranging between 10% and 50% using two different emulsification techniques: magnetic stirring and high pressure homogenization (HPH) (Figure 8a). Prior to cross-linking, we determine the droplet size in emulsions prepared with both techniques. The sizes of droplets emulsified by magnetic stirring are around 130 μm in diameter with a COV of 60%, whereas emulsion droplets prepared by HPH are approximately 0.72 μm in diameter with a COV of 22%. The loading of FEN increases with increasing volume fraction as expected in samples prepared with both emulsification techniques (Figure 8a). However, the error bars in measured loading are significantly smaller with HPH as compared to magnetic stirring. Large variations in API loading are undesired in the pharmaceutical industry as they directly affect the dosage consistency and reproducibility. We hypothesize that the large variation in loading might be due to the relatively large mean droplet diameter and the polydispersity characteristic of magnetic stirring. Magnetic stirring is a cheap yet crude emulsification technique that results in relatively large droplets with large size distributions. These large variations in loading can be understood in terms of terminal velocity (V_t). The terminal velocity of a drop of diameter (d) and density of ρ_d creaming in surrounding medium of density ρ_c and viscosity μ is given by $V_t \approx (d^2(\rho_d - \rho_c)/\mu)$ using the creeping flow assumption. The larger droplets cream faster in the finite time required for transferring the emulsified sample after its homogenization to the dripping processes described in the Materials and Methods. The creaming of emulsions droplets in precross-linked solution generates gradients in amounts of encapsulated emulsions, and hence loading among cross-linked ALG beads. The emulsions prepared by HPH are called nanoemulsions, and they have both smaller droplet diameter and polydispersity.[38,52] As is evident from ESEM images given in Figure 7b, the size of the nanoemulsion droplets did not change after cross-linking. Furthermore, nanoemulsions are commonly used in the cosmetics, food, and pharmaceutical industry due to their long-term stability. Hence, we identify HPH as an optimum emulsification method for our purpose.

Second, we investigate which solvent is more suitable for preparing emulsion-laden hydrogels and how we can optimize loading, a critical parameter in industrial practice. The loading is a function of the ALG concentration in the continuous phase (C_{ALG}), the concentration of API dissolved in the dispersed phase (C_{API}), and the volume fraction of the dispersed phase in continuous phase (φ). A rational optimization is required for designing emulsion-laden hydrogels to achieve maximum loading. The maximum φ that can be used is dictated by how densely emulsions can be packed.[38] The maximum C_{API} is

dx.doi.org/10.1021/cg500250e | Cryst. Growth Des. XXXX, XXX, XXX−XXX

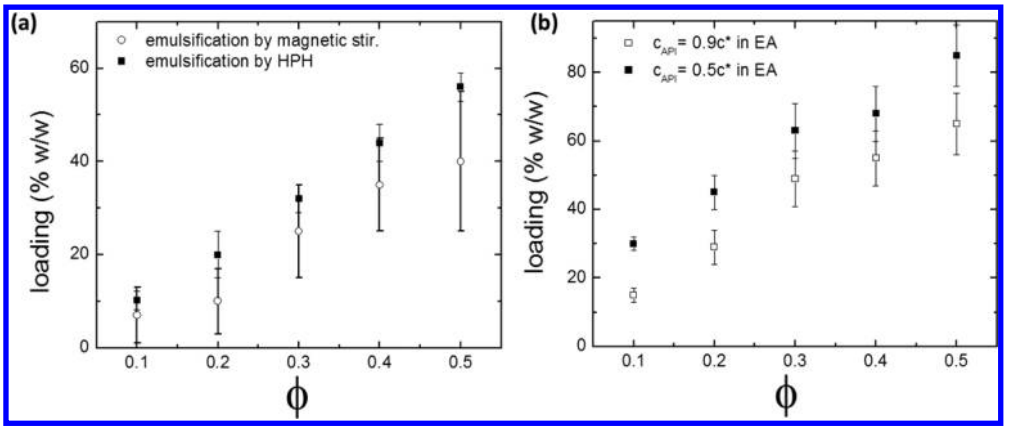

Figure 8. (a) Loading (% weight by weight) of FEN in emulsion-laden hydrogels prepared by different emulsification techniques. (b) Loading (% weight by weight) of FEN in ethyl acetate with two FEN concentrations for varying emulsion volume fractions measured by evaporation method.

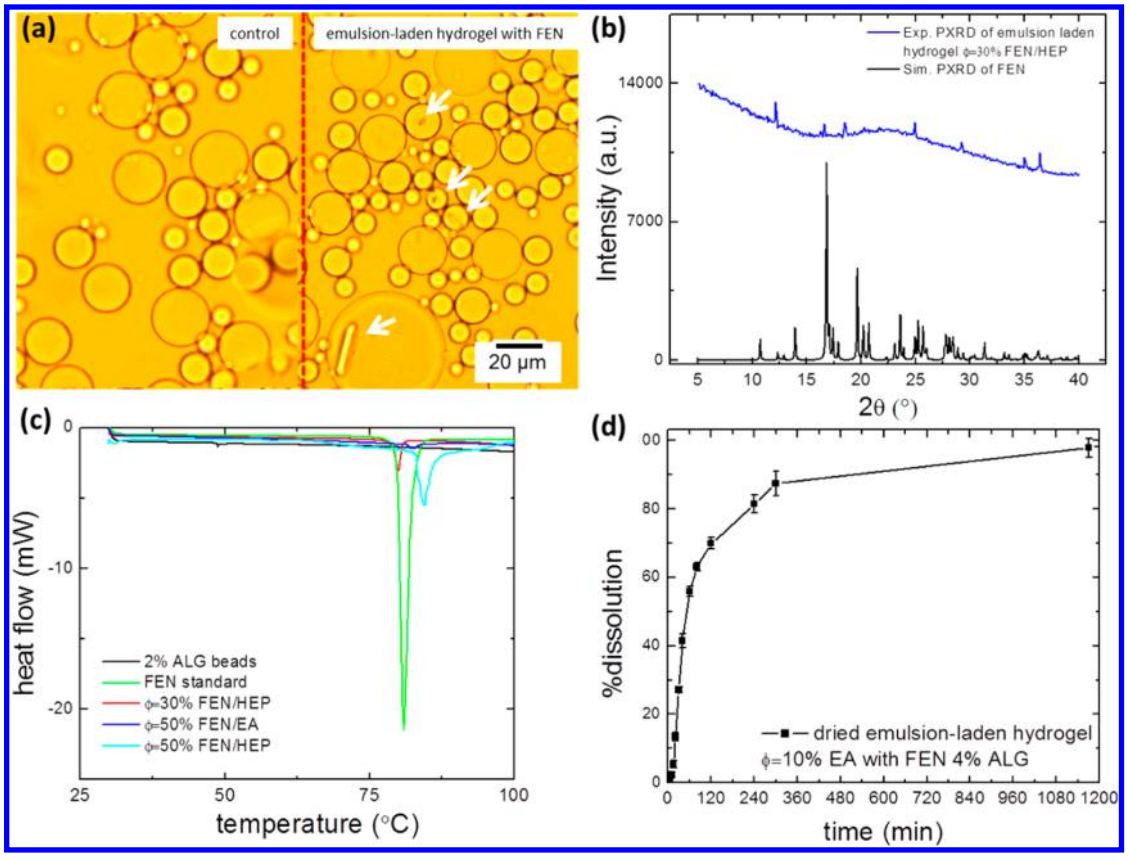

Figure 9. Confirmation of FEN crystallization inside emulsion-laden hydrogels. Panel (a): the control, emulsion droplets encapsulated in 2% ALG matrix prepared by magnetic stirring without FEN and with FEN. FEN crystals growing inside emulsion droplets carrying FEN are observed. Both samples have been cooled to 10 °C, and time lapse images are taken. Panel (a) shows images taken at t = 4 h. Details on sample preparation appear in the Supporting Information. Panel (b) shows PXRD data of API loaded emulsion-laden hydrogels prepared by HPH emulsification. Panel (c) shows the DSC data for FEN loaded hydrogels with both HEP and EA. Panel (d) shows the dissolution profile of dried emulsion-laden hydrogels.

dictated by the solubility of FEN in the dispersed organic phase. The solubility of FEN in heptane is slightly above 9 mg/mL at 25 °C. The solubility (c*) of FEN in EA is significantly larger, 600 mg/mL. Furthermore, EA has a low vapor pressure at room temperature, which makes it an ideal candidate for effectively removing residual solvent. As expected, we managed to load larger amounts of FEN with EA as compared to HEP (Figure 8a,b). However, we observed undesired precipitation of FEN in precross-linked emulsion. We believe this precipitation is due to moderate solubility of EA in water. We counteracted this by reducing the concentration of FEN below its saturation value (c_{API} = 0.5c* and 0.9c*). By reducing the concentration of FEN in emulsion droplets, we effectively decrease the amount of FEN precipitating and thus reached relatively high loading values (~80%).

Furthermore, other process and product parameters need to be taken into account while designing API-carrying emulsion-laden hydrogels. For instance, at high volume fractions (φ > 50%), cross-linking of emulsion by the dripping method becomes extremely difficult due to the high viscosity and the

dx.doi.org/10.1021/cg500250e | Cryst. Growth Des. XXXX, XXX, XXX−XXX

jamming of emulsions in the dripping needle. Another critical product parameter is the mechanical integrity of hydrogel beads, which is influenced by C_{ALG} and φ. At low C_{ALG} and high φ, the hydrogel easily breaks and disintegrates.

Through systematic investigation of solvent types and emulsification methods, we designed an emulsion-laden hydrogel formulation that can carry industrially relevant amounts of a model hydrophobic API. The next step is to check if the emulsion-laden hydrogels can crystallize FEN. To identify whether the FEN encapsulated inside the ALG matrix is crystalline or amorphous, three characterization techniques are employed: optical microscopy, PXRD, and differential scanning calorimetry (DSC). For optical microscopy, we prepared emulsion-laden hydrogel sandwiched between two glass slides (see the Supporting Information for detailed procedure). We have chosen to prepare emulsions with magnetic stirring so that the large size of droplets will enable light microscopy. The sample is cooled to 10 °C on a microscope stage and imaged using time-lapse microscopy. After 4 h, we observed FEN crystals particularly in large droplets as shown in Figure 9a, whereas the control with emulsion droplets containing no API did not show crystallization. This observation proves that FEN can be crystallized inside emulsion-laden hydrogels. The experimental diffractogram of FEN carrying emulsion-laden ALG particles prepared by HPH indicates that crystals of FEN have formed inside the ALG hydrogels (Figure 9b). The intensity of the diffraction in the peaks present is not high enough to determine the percent of crystallinity, and therefore further analysis with DSC is required. Thermographs are obtained using empty ALG beads, an FEN standard, and ALG beads loaded with FEN at different volume fractions with different solvents (HEP and EA) in Figure 9c. From these thermographs, it can be concluded that FEN loaded into both HEP and EA during this investigation produces crystalline FEN. Crystalline FEN standards and FEN-loaded emulsion-laden hydrogels all produce melting endotherms at ∼78 °C, demonstrating the existence of crystalline FEN within. We also looked at the dissolution behavior of dried emulsion-laden hydrogels. We observed that 80% of the FEN dissolved within 4 h followed by a slower release rate. This two-stage release profile is observed in other polymeric delivery mechanisms as well.

In this study, we investigated the utility of ALG hydrogels as a versatile biocompatible vehicle for crystallizing and encapsulating APIs that exhibit dramatically different solubilities in water due to their distinct chemical structures. For hydrophilic model API (ACM), we investigated the potential of ALG hydrogels as heteronucleants to influence nucleation induction times from solution and their ability to encapsulate ACM. Our results indicate that a cutoff in ALG concentration (hence hydrogel mesh size) exists in which ALG particles of different concentrations are able to promote the nucleation of ACM from solution. Below this cutoff, ALG particles suppress the nucleation. We attribute these results to the interplay between the mesh-size-induced confinement and the solute−polymer interactions. Furthermore, the amount of ACM that can be loaded into hydrogels through thermodynamic partitioning depends on mesh size. Hence, a trade-off is required to design ALG hydrogels capable of functioning as heteronucleants in a crystallization process while carrying large amounts of the model hydrophilic API. For the hydrophobic API, FEN, we demonstrated efficient loading (∼up to 82% w/w) and crystallization of FEN in emulsion-laden hydrogels. We identified the optimum emulsification method, solvent type, volume fraction of dispersed phase, and concentration of API within the dispersed phase to maximize loading. Our results suggest that emulsion-laden ALG hydrogels prepared with high pressure homogenization utilizing ethyl acetate as the dispersed phase might offer fine control over dosage and dosage consistency while achieving significant loading of FEN. The methodologies presented open new investigation alleys for designing biocompatible materials that can act as heteronucleants while encapsulating large amounts of drugs with vastly different water solubilities. Furthermore, ALG hydrogels and emulsion-laden hydrogels can be used as final drug formulation in a continuous manufacturing scheme due to their biocompatible nature and their ability to carry APIs with diverse chemical nature.

■ ASSOCIATED CONTENT

Supporting Information

Detailed experimental procedures, rheological determination of ALG mesh size, thermogravimetric analysis (TGA), induction time analysis, and tablet preparation. This material is available free of charge via the Internet at http://pubs.acs.org.

■ AUTHOR INFORMATION

Corresponding Author

*E-mail: pdoyle@mit.edu.

Author Contributions

†These authors contributed equally.

Notes

The authors declare no competing financial interest.

■ ACKNOWLEDGMENTS

We acknowledge the Novartis-MIT Continuous Manufacturing Center for financial support. H.B.E. acknowledges R. Shaw from MIT UROP program, and A. Ryan from MIT machine shop for their support with the experiments.

■ REFERENCES

(1) Debenedetti, P. G. *Metastable Liquids: Concepts and Principles*; Princeton University Press: Princeton, NJ, 1996.

(2) Mullin, J. W. *Crystallization*, 4th ed.; Butterworth-Heinemann: Boston, 2001.

(3) Oxtoby, D. W. Nucleation of first-order phase transitions. *Acc. Chem. Res.* **1998**, *31* (2), 91−97.

(4) Price, C. P.; Grzesiak, A. L.; Matzger, A. J. Crystalline polymorph selection and discovery with polymer heteronuclei. *J. Am. Chem. Soc.* **2005**, *127*, 5512−5517.

(5) Berman, A.; Ahn, D. J.; Lio, A.; Salmeron, M.; Reichert, A.; Charych, D. Total alignment of calcite at acidic polydiacetylene films - Cooperativity at the organic-inorganic interface. *Science* **1995**, *269*, 515−518.

(6) Aizenberg, J.; Black, A. J.; Whitesides, G. H. Oriented growth of calcite controlled by self-assembled monolayers of functionalized alkanethiols supported on gold and silver. *J. Am. Chem. Soc.* **1999**, *121*, 4500−4509.

(7) Aizenberg, J.; Black, A. J.; Whitesides, G. M. Control of crystal nucleation by patterned self-assembled monolayers. *Nature* **1999**, *398*, 495−498.

(8) Bunker, B. C.; Rieke, P. C.; Tarasevich, B. J.; Campbell, A. A.; Fryxell, G. E.; Graff, G. L.; Song, L.; Liu, J.; Virden, J. W.; Mcvay, G. L. Ceramic thin-film formation on functionalized interfaces through biomimetic processing. *Science* **1994**, *264*, 48−55.

(9) Lee, A. Y.; Lee, I. S.; Dettet, S. S.; Boerner, J.; Myerson, A. S. Crystallization on confined engineered surfaces: A method to control

crystal size and generate different polymorphs. *J. Am. Chem. Soc.* **2005**, *127*, 14982−14983.
(10) Carter, P. W.; Ward, M. D. Topographically directed nucleation of organic-crystals on molecular single-crystal substrates. *J. Am. Chem. Soc.* **1993**, *115*, 11521−11535.
(11) Gavish, M.; Wang, J. L.; Eisenstein, M.; Lahav, M.; Leiserowitz, L. The role of crystal polarity in alpha-amino-acid crystals for induced nucleation of ice. *Science* **1992**, *256*, 815−818.
(12) Hiremath, R.; Basile, J. A.; Varney, S. W.; Swift, J. A. Controlling molecular crystal polymorphism with self-assembled monolayer templates. *J. Am. Chem. Soc.* **2005**, *127*, 18321−18327.
(13) Page, A. J.; Sear, R. P. Heterogeneous nucleation in and out of pores. *Phys. Rev. Lett.* **2006**, *97*, 065701.
(14) Page, A. J.; Sear, R. P. Crystallization controlled by the geometry of a surface. *J. Am. Chem. Soc.* **2009**, *131*, 17550−17551.
(15) Ha, J. M.; Wolf, J. H.; Hillmyer, M. A.; Ward, M. D. Polymorph selectivity under nanoscopic confinement. *J. Am. Chem. Soc.* **2004**, *126*, 3382−3383.
(16) Beiner, M.; Rengarajan, G. T.; Pankaj, S.; Enke, D.; Steinhart, M. Manipulating the crystalline state of pharmaceuticals by nano-confinement. *Nano Lett.* **2007**, *7*, 1381−1385.
(17) Rengarajan, G. T.; Enke, D.; Steinhart, M.; Beiner, M. Stabilization of the amorphous state of pharmaceuticals in nanopores. *J. Mater. Chem.* **2008**, *18*, 2537−2539.
(18) Diao, Y.; Whaley, K. E.; Helgeson, M. E.; Woldeyes, M. A.; Doyle, P. S.; Myerson, A. S.; Hatton, T. A.; Trout, B. L. Gel-induced selective crystallization of polymorphs. *J. Am. Chem. Soc.* **2012**, *134*, 673−684.
(19) Diao, Y.; Helgeson, M.; Doyle, P.; Myerson, A.; Hatton, T. A.; Trout, B. Design of polymeric substrates for controlled molecular crystallization. *Abstr. Pap. Am. Chem. Soc.* **2011**, 242.
(20) Diao, Y.; Helgeson, M. E.; Siam, Z. A.; Doyle, P. S.; Myerson, A. S.; Hatton, T. A.; Trout, B. L. Nucleation under soft confinement: Role of polymer-solute interactions. *Cryst. Growth Des.* **2012**, *12*, 508−517.
(21) Eral, H. B.; Mugele, F.; Duits, M. H. G. Colloidal dynamics near a particle-covered surface. *Langmuir* **2011**, *27*, 12297−12303.
(22) Eral, H. B.; Oh, J. M.; van den Ende, D.; Mugele, F.; Duits, M. H. G. Anisotropic and hindered diffusion of colloidal particles in a closed cylinder. *Langmuir* **2010**, *26*, 16722−16729.
(23) Williams, I.; Oguz, E. C.; Bartlett, P.; Lowen, H.; Royall, C. P. Direct measurement of osmotic pressure via adaptive confinement of quasi hard disc colloids. *Nat. Commun.* **2013**, *4*, 2555.
(24) Oguz, E. C.; Marechal, M.; Ramiro-Manzano, F.; Rodriguez, I.; Messina, R.; Meseguer, F. J.; Lowen, H. Packing confined hard spheres denser with adaptive prism phases. *Phys. Rev. Lett.* **2012**, *109*, 218301.
(25) Suleimanov, Y. V. Surface diffusion of hydrogen on Ni(100) from ring polymer molecular dynamics. *J. Phys. Chem. C* **2012**, *116*, 11141−11153.
(26) Diao, Y.; Helgeson, M. E.; Myerson, A. S.; Hatton, T. A.; Doyle, P. S.; Trout, B. L. Controlled nucleation from solution using polymer microgels. *J. Am. Chem. Soc.* **2011**, *133*, 3756−3759.
(27) Jackson, C. L.; McKenna, G. B. Vitrification and crystallization of organic liquids confined to nanoscale pores. *Chem. Mater.* **1996**, *8*, 2128−2137.
(28) Augst, A. D.; Kong, H. J.; Mooney, D. J. Alginate hydrogels as biomaterials. *Macromol. Biosci.* **2006**, *6*, 623−633.
(29) Martinsen, A.; Skjakbraek, G.; Smidsrod, O. Alginate as immobilization material. 1. Correlation between chemical and physical-properties of alginate gel beads. *Biotechnol. Bioeng.* **1989**, *33*, 79−89.
(30) Moe, S. T.; Elgsaeter, A.; Skjakbraek, G.; Smidsrod, O. A new approach for estimating the cross-link density of covalently cross-linked ionic polysaccharide gels. *Carbohydr. Polym.* **1993**, *20*, 263−268.
(31) Moe, S. T.; Skjak-Braek, G.; Smidsrod, O. Covalently cross-linked sodium alginate beads. *Food Hydrocolloids* **1991**, *5*, 119−123.
(32) Strand, B. L.; Morch, Y. A.; Skjak-Braek, G. Alginate as immobilization matrix for cells. *Minerva Biotecnol.* **2000**, *12*, 223−233.
(33) Takka, S.; Acarturk, F. Calcium alginate microparticles for oral administration: I: effect of sodium alginate type on drug release and drug entrapment efficiency. *J. Microencapsulation* **1999**, *16*, 275−290.
(34) Lipinski, C. A.; Lombardo, F.; Dominy, B. W.; Feeney, P. J. Experimental and computational approaches to estimate solubility and permeability in drug discovery and development settings. *Adv. Drug Delivery Rev.* **2012**, *64*, 4−17.
(35) Inoue, T.; Chen, G. H.; Hoffman, A. S.; Nakamae, K. A hydrophobically modified bioadhesive polymeric carrier for controlled drug delivery to mucosal surfaces. *J. Bioact. Compat. Polym.* **1998**, *13*, 50−64.
(36) Gou, M. L.; Li, X. Y.; Dai, M.; Gong, C. Y.; Wang, X. H.; Xie, Y.; Deng, H. X.; Chen, L. J.; Zhao, X.; Qian, Z. Y.; Wei, Y. Q. A novel injectable local hydrophobic drug delivery system: Biodegradable nanoparticles in thermo-sensitive hydrogel. *Int. J. Pharm.* **2008**, *359*, 228−233.
(37) Jeong, B.; Bae, Y. H.; Kim, S. W. Drug release from biodegradable injectable thermosensitive hydrogel of PEG-PLGA-PEG triblock copolymers. *J. Controlled Release* **2000**, *63*, 155−163.
(38) Mason, T. G.; Wilking, J. N.; Meleson, K.; Chang, C. B.; Graves, S. M. Nanoemulsions: formation, structure, and physical properties. *J. Phys.: Condens. Matter* **2006**, *18*, R635−R666.
(39) McClements, D. J. Crystals and crystallization in oil-in-water emulsions: Implications for emulsion-based delivery systems. *Adv. Colloid Interface Sci.* **2012**, *174*, 1−30.
(40) McClements, D. J. Nanoemulsions versus microemulsions: terminology, differences, and similarities. *Soft Matter* **2012**, *8*, 1719−1729.
(41) An, H. Z.; Helgeson, M. E.; Doyle, P. S. Nanoemulsion composite microgels for orthogonal encapsulation and release. *Adv. Mater.* **2012**, *24*, 3838−3844.
(42) Jagadeesan, D.; Nasimova, I.; Gourevich, I.; Starodubtsev, S.; Kumacheva, E. Microgels for the encapsulaption and stimulus-responsive release of molecules with distinct polarities. *Macromol. Biosci.* **2011**, *11*, 889−896.
(43) Josef, E.; Zilberman, M.; Bianco-Peled, H. Composite alginate hydrogels: An innovative approach for the controlled release of hydrophobic drugs. *Acta Biomater.* **2010**, *6*, 4642−4649.
(44) Turco, G.; Donati, I.; Grassi, M.; Marchioli, G.; Lapasin, R.; Paoletti, S. Mechanical spectroscopy and relaxometry on alginate hydrogels: A comparative analysis for structural characterization and network mesh size determination. *Biomacromolecules* **2011**, *12*, 1272−1282.
(45) Larson, R. *The Structure and Rheology of Complex Fluids*; Oxford University Press: New York, 1999.
(46) Gardel, M. L.; Shin, J. H.; MacKintosh, F. C.; Mahadevan, L.; Matsudaira, P.; Weitz, D. A. Elastic behavior of cross-linked and bundled actin networks. *Science* **2004**, *304*, 1301−1305.
(47) Flory, P. J. *Principles of Polymer Chemistry*; Oxford University Press: Ithaca, NY, 1953.
(48) Chan, A. W.; Whitney, R. A.; Neufeld, R. J. Kinetic controlled synthesis of pH-responsive network alginate. *Biomacromolecules* **2008**, *9*, 2536−2545.
(49) Jamzad, S.; Fassihi, R. Role of surfactant and pH on dissolution properties of fenofibrate and glipizide - A technical note. *AAPS PharmSciTech* **2006**, *7*, E33.
(50) Diao, Y.; Harada, T.; Myerson, A. S.; Hatton, T. A.; Trout, B. L. The role of nanopore shape in surface-induced crystallization. *Nat. Mater.* **2011**, *10*, 867−871.
(51) Diao, Y.; Helgeson, M.; Myerson, A.; Hatton, T. A.; Doyle, P.; Trout, B. Rational design of polymeric nucleants for controlling nucleation. *Abstr. Pap. Am. Chem. Soc.* **2011**, 241.
(52) Fryd, M. M.; Mason, T. G. Advanced nanoemulsions. *Annu. Rev. Phys. Chem.* **2012**, *63*, 493−518.